Journal of Geodesy (2026) 100:6
https://doi.org/10.1007/s00190-025-02013-w

ORIGINAL ARTICLE

The annual variation of the M2 gravimetric tidal parameters investigated with nonlinear, time-stepping ocean models

E. Schroth[1,3] · T. Forbriger[2] · M. Westerhaus[3] · M. Müller[4] · J. Saynisch-Wagner[5] · B. K. Arbic[6] · K. Drach[3,7] · M. Thomas[5,11] · U. Gräwe[8] · J. F. Shriver[9] · A. Mehra[10]

Received: 4 March 2025 / Accepted: 9 October 2025

Abstract

Temporal variations of the M2 tidal parameters in gravity are observed at all superconducting gravimeter stations. We specifically investigate the annual variation of M2 tidal parameters. A similar variation is observed for the parameters from sea surface heights which is larger than expected from astronomical forcing alone. This leads to the hypothesis that the variations of the gravimetric tidal parameters are caused by the loading of the annual variation of M2 in the oceans. Only nonlinear, time-stepping ocean models are able to describe such variations. We use sea surface heights from three global and two regional models of this kind to calculate the loading. The loading time series is then added to synthetic body tides and analyzed by a moving window tidal analysis with ETERNA in the same way as the measured data. We compare the resulting variations of the M2 tidal parameters for synthetic gravity with those observed from measurements. Three of the five ocean models show an annual variation of a similar order of magnitude which supports our hypothesis. The other two ocean models produce smaller or no clear annual variation of the M2 tidal parameters. In the ocean the annual variation of M2 has large amplitudes in shelf areas and small amplitudes in the open ocean. Large areas with small amplitude might contribute to the gravity loading as much as small areas with large amplitudes do. We investigate this with the global Hycom model at three SG stations. The investigation shows that not only close shelf areas but also distant ocean regions, including open ocean areas, contribute significantly to the annual variation of the M2 tidal parameters at the superconducting gravimeter stations.

Keywords Tidal analysis · Earth tides · Ocean tides · Ocean models · Time variable gravimetry und superconducting gravimetry

1 Introduction

Tides are constantly probing the Earth. Measurements of Earth's response to tides enables understanding of Earth's internal structure and in theory its changes with time. The large-scale properties of the solid Earth which are crucial for its response to tides in gravity are assumed to change slowly (on geological time scales), whereas ocean and atmospheric

At the time when the study was made Eva Schroth was member of the KIT. She works now at the Federal Agency of Cartography and Geodesy. K. Drach: Konstantin Drach is employed at the university of Tübingen. When he worked or this study he was member of the KIT.

✉ E. Schroth
eva.schroth@bkg.bund.de

1 Geodetic Observatory Wettzell, Federal Agence for Cartography and Geodesy, Bad Kötzting, Germany

2 Geophysical Institute, Black Forest Observatory, Karlsruhe Institute of Technology, Schiltach, Germany

3 Geodetic Institute, Karlsruhe Institute of Technology, Karlsruhe, Germany

4 Norwegian Meteorological Institute, Oslo, Norway

5 GFZ Helmholtz Centre for Geosciences, Earth System Modelling Potsdam, Germany

6 Department of Earth and Environmental Sciences, University of Michigan, Ann Arbor, MI, USA

7 Department of Geosciences Hydrogeology, University of Tübingen, Tübingen, Germany

8 Leibniz-Institute for Baltic Sea Research, Warnemünde, Germany

9 Naval Research Laboratory, Oceanography Division, Stennis Space Center, Hancock County, MS, USA

10 Ocean Prediction Center, National Centers for Environmental Prediction, NOAA, College Park, USA

11 Freie Universität, Institute for Meteorology, Berlin, Germany

Published online: 22 January 2026

tides exhibit quicker variations. Because the propagation of tidal waves in these parts of the Earth system depends on boundary conditions that are governed by seasons and climate, tides in the atmosphere and oceans vary on these time scales. In the context of tidal analysis of gravity data measured by superconducting gravimeters (SG), the different parts of the Earth system are coupled by loading effects. Thus, any variation in oceanic and atmospheric tides can lead to apparent temporal variations of the solid Earth response. These complex interrelations have to be thoroughly understood if tides are used as an ever-present test signal which may, for example, be applied to search for temporal changes of the deformability of the crust at continental margins (e. g. Westerhaus 1997) or to characterize aquifers with tilt and strain tides. A prominent example for temporal variations is the apparent annual periodicity of the solid Earth's response to the principal semidiurnal lunar constituent M2. Modern SGs produce data of unprecedented accuracy and precision such that observed variations are significant with respect to the standard deviation of tidal parameters as obtained from data residuals. Such variations are demonstrated by Meurers (2004); Meurers et al. (2016); Jahr (2015); Schroth (2013) and Schroth et al. (2018). Instrumental causes like a changing calibration factor of the SG were discussed in previous studies and ruled out (e. g. Meurers et al. 2016; Schroth et al. 2018). Given that changes of the admittance of Earth's body to tidal forces within a few months are unlikely, we must search for alternative explanations of this phenomenon. We hypothesize that annual changes of the loading due to corresponding variations of the M2 amplitude in the ocean cause the observed annual variation of the M2 parameters of tidal gravity (hereafter referred to as AVM2).

1.1 Previous studies

The annual variation of the M2 tide in the sea surface height (hereafter referred to as AVM2ssh to be distinguished from the corresponding AVM2 for gravity data; sea surface height referred to as SSH) was already observed in the 1930 s by Corkan (1934) in tide gauge data. These observations were corroborated in subsequent years for different places on Earth (e. g. Foreman et al. 1995). Huess and Andersen (2001) observed an AVM2ssh in satellite altimeter data from the North Sea. The effects causing the AVM2ssh were for example studied by Kang et al. (2002). They suggest a seasonally varying stratification to be the cause for the variation. Müller (2012) and Müller et al. (2014) extended the investigations to a global scale and identified a temporally varying loss of energy to turbulent processes and friction as the driving mechanism. This energy loss acts on the barotropic tidal transport and finally influences amplitude and phase of the corresponding tide. Müller et al. (2014) showed that an ocean model with barotropic and baroclinic tides and climatologic atmospheric forcing, exhibits AVM2ssh of several centimeters in shelf areas, similar to variations observed with tide gauges and altimeters.

The loading, as we define the term for this study, is the combined effect of the deformation of the Earth's crust by the ocean masses and their Newtonian attraction on tilt or gravity measurements at an inland station. The influence of an AVM2ssh in the oceans on tiltmeters in Great Britain was studied by Baker and Alcock (1983). They observed a corresponding periodicity in analysis results of tide gauge data and tilt measurements. A similar observation was made for the comparison of tidal parameters obtained for SG data and tide gauge data in Ny-Alesund by Sato et al. (2006). Merriam (1995) found significant contributions in the residuals of a tidal analysis (based on the response method) of data from the SG in Cantley at frequencies at which nonlinear tides are reported in the Bay of Fundy, including an AVM2 signal.

1.2 Objectives of the study

Correcting tidal parameters from the time-invariant ocean loading with the help of ocean tide models based on altimeter data is a standard procedure in tidal research. These models are computed in the frequency domain and are constant with time. They do not contain an AVM2ssh signal. Nevertheless this kind of ocean model describes the time-invariant component of the ocean tides relatively well. The novelty of the present study is that nonlinear, time-stepping ocean models calculating barotropic and baroclinic tides under tidal and atmospheric forcing are used to quantify time variable gravity loading at SG stations within the continents. We assess how far a validated ocean model can generate variations in the M2 tidal parameters and determine the regions of the global oceans that significantly contribute to the AVM2.

2 Approach and methods

2.1 Approach

As mentioned in Sect. 1.2, corrections of tidal parameters for the time-invariant loading are commonly used in investigations of gravity tides. Baker and Bos (2003) compare the performance of different such models. Other than the time-invariant models, the time-stepping models cannot yet be considered to predict the real oceans precisely enough for a correction of gravity tides. They were developed to study ocean physics rather than to deliver operational forecasts of water levels (see Sect. 4).

We, therefore, calculate a loading time series from the nonlinear, time-stepping ocean models' output and add it to a synthetic body tides gravity signal. In a tidal analysis (see Sect. 2.2) of data sets longer than approx. 1 year an annual

variation of M2 can be described by the estimation of the tidal parameters of the satellite constituents $\alpha 2$ and $\beta 2$ (see Sect. 5.1). Analyses like this were shown for example by Meurers et al. (2016). Although some years of data are available from the ocean models we decided to study the effect with moving window tidal analysis (MWA, see Sect. 2.2). The AVM2ssh is driven by meteorology. Therefore, it does not behave strictly periodically and appears with different amplitudes from year to year. This can be well observed in the time-dependent tidal parameters from MWA, in contrast to residuals from a tidal analysis.

After carrying out a MWA on the combined signal, the time-dependent tidal parameters are compared to the results obtained from measured gravity data with the same method. We call this approach 'synthetic data MWA', in the following. Our approach has the advantage that the source of the observed variations can be clearly identified: The ETERNA earth tide analysis and prediction package (Wenzel 1996) provides predictions of gravity tides for given tidal parameters at the specified location and time based on tidal potential catalogues as well as analyses of tidal data by the Least-squares adjustment method. Both parts, prediction and analysis, are consistent. If the synthetic body tides are analyzed with the same settings (e.g., wave grouping, see Sect. 2.2) as used for their prediction, the gravimetric factor and phase from MWA are constant (Schroth 2013). Variations of the tidal parameters obtained with synthetic data MWA can therefore only be caused by the AVM2ssh loading time series. We then analyze parameter time series of modeled and measured data and scrutinize potential similarities with respect to our hypothesis that the AVM2ssh is the source of the observed variations of the M2 tidal parameters. However, as mentioned above, we do not expect a one by one matching of model and observation results. Therefore, we focus on a visual comparison of magnitudes and character (the period and the order of magnitude) of the parameter variations and evaluate the plausibility of the postulated causal relationship between annual variations of M2 gravimetric factor and phase from SG-data in a heuristic manner.

2.2 Tidal analysis and moving window analysis

To investigate the temporal variation of time-variable tidal parameters, we use the technique of moving window analyses. In a moving window tidal analysis, the entire time series is subdivided into segments of 90 days length, which appear at intervals of 2 days and overlap by 88 days. The tidal analysis results for all segments yield a time series for each tidal parameter. We use a modified version of the software ETERNA 3.4 (program analyze, Wenzel et al. 2022), which determines amplitudes and phases of tidal constituents by fitting the body tide model to the measured data in a least-squares-approach. The wave groups for which the tidal parameters are estimated are given in Table 4 in Appendix E. A model for an elliptical, uniformly rotating Earth with liquid inner core and viscous mantle (Wahr-Dehant-Zschau model, Dehant 1987) is used as reference. We implemented a free core nutation (FCN) period of 431.39 sidereal days (Dehant et al. 1999) to replace the outdated resonance model of the original ETERNA version. The analysis results are a gravimetric factor, i.e., the ratio of the observed and the forcing amplitude of a tidal constituent, as well as the corresponding phase lead. The resulting tidal parameters for each segment are plotted over the centroid time of the corresponding window. A band-pass FIR-filter from 1 cpd to 5 cpd was applied to data and analysis model. The analysis uses a Hanning taper and includes local air pressure as an additional regressor. Wave groups are assembled as recommended by Wenzel (1997a) (see also Schroth et al. 2018, Table 5) for time series of less than six months. Wave groups Q1 and higher (frequency $>$ approx. 0.5 cpd) are used. A comprehensive description of the analysis approach as well as an extensive catalogue of gravimetric factor and phase variations for 19 European and global SG stations is given by Schroth et al. (2018).

In all subsequent figures displaying temporal behavior, the standard deviations for the tidal parameters as estimated by ETERNA 3.4 are indicated by the thickness of the measured parameter curves. Please note that formal errors of the least-squares-adjustment, often interpreted as standard deviations, are in general too optimistic and not a proper measure of the tidal parameter's precision (Wenzel 1997a, b). In the case of synthetic data MWA standard deviations are just a measure of the similarity between synthetic tidal gravity with and without loading. Synthetic data does not contain statistical noise. To enhance comparability of the temporal variations, the mean value representing the time-invariant part of the tidal parameters is subtracted from all MWA results. These signal components are discussed exemplarily for the Black Forest Observatory (BFO) in Appendix D. They give an impression of how well the ocean model predicts the time-invariant M2 amplitude.

2.3 Ocean loading

Our approach of synthetic data MWA as described in Sect. 2.1 requires the calculation of the gravity loading $l(t)$ from the ocean models' output. This is expressed by the commonly used integral

$$l(t) = \rho \iint_{\text{oceans}} G(|\vec{r} - \vec{r}'|)\, h(t, \vec{r}')\, \mathrm{d}A \tag{1}$$

which was introduced by Farrell (1972). The water density $\rho = 1031\,\mathrm{kg\,m^{-3}}$ is assumed to be constant. The height h is given by the SSH values from the ocean models and the areas

around the model grid points dA are approximated as rectangles on a spherical surface with side length of half the distance to the neighboring grid points in the latitude and longitude directions. $G(|\vec{r}-\vec{r}'|)$ is the Green's function for the distance $(|\vec{r}-\vec{r}'|)$. We used the values of Green's function provided by Na and Baek (2011). As the Green's functions are required for specific distances, the given values were interpolated by piecewise cubic Hermite interpolating polynomials (PCHIP, as implemented in MATLAB). Tests showed that the interpolation results are more accurate when the Green's functions are first normalized by the distance $d = |\vec{r} - \vec{r}'|$.
All calculations were done with MATLAB.[1] To reduce computation time, we neglect the altitude of the gravimeter stations and the coast lines that may intersect grid cells of the ocean model. The coast line is taken as defined by the ocean models which distinguish between on-shore and off-shore grid cells. We also do not interpolate over the grid cell's extent. In order to ensure that this is of insignificant influence for the AVM2, we compared our simplified approach with the software package 'Some Programs for Ocean Tide Loading' (SPOTL, Agnew 2012)for example stations (see Sect. B in the Appendix). The variations of the tidal parameters do not differ significantly.

3 Gravity data

We use data recorded by globally distributed superconducting gravimeters (SG). The selected stations are shown in Fig. 1. Most of the data were downloaded from the International Geodynamics and Earth Tide Service (IGETS) database.[2] Preprocessed hourly data (Voigt et al. 2016, level 2 products) are used. For BFO, the IGETS data set was complemented by additional data obtained from the local data archive. The data set from Onsala was provided by the station operators (H.-G. Scherneck, pers. comm.). For dual-sphere instruments (marked with an asterisk in Table 1) the data from the lower sensor are used, because this is better shielded against magnetic disturbances (Zürn et al. 2008).
The synthetic body tides are calculated with *predict* (Wenzel 1996). Using exactly the same wave groups for calculating synthetic body tides as in the analysis, it is assured that no variations of the tidal analysis parameters are caused by the synthetic body tides (see Sect. 2.1). The values $\delta = 1.16$ and $\varphi = 0°$ are assumed for most of the wave groups in the computation of synthetic gravity time series. Only for K1, δ is set to 1.13 and for M3M6, δ is set to 1.06 (see Table 4 in the Appendix for definition of wave groups). These values are close to the theoretical tidal parameters calculated based on Earth models obtained from seismology (Dehant et al. 1999). We do not use the exact numbers because these values are just easier to handle. The small difference between the theoretical values and the number used here is not relevant for the interpretation of our results because we subtract the mean values at any rate.

Table 1 SG data sets. Name and abbreviation of the station and length of the data set. Dual-sphere instruments are marked with an asterisk. Data in the specified time intervals usually contain gaps. The number and size of gaps are individual for each station

Station	Length
BF: Black Forest Observatory*, Germany	2009–2016
CA: Cantley, Canada	1997–2013
CB: Canberra, Australia	1997–2015
MB: Membach, Belgium	1997–2011
MO: Moxa*, Germany	2000–2014
OS: Onsala, Sweden	2009–2018
SU: Sutherland*, South Africa	2000–2014
TC: TIGO Concepción, Chile	2003–2014

4 Ocean models

We use results from the real-time ocean forecast system (*ARTOFS*, Mehra and Rivin 2010), the *Stormtide* model (Müller et al. 2014), the ocean model for circulation and tides (*OMCT*, Thomas et al. 2001; Dobslaw et al. 2013), the HYbrid Coordinate Ocean model (*HGT*, Arbic et al. 2010, 2012) and the *North Sea* model (Gräwe et al. 2015) for the computation of loading. All of them contain barotropic and baroclinic tides, have an astronomical tidal forcing (except for the *North Sea* model) as well as an atmospheric forcing. They differ with respect to spatial extent, spatial resolution, implemented phenomena and boundary conditions. Concerning tidal forcing, two different representations for tidal forcing are applied: *Stormtide* and *OMCT* use the ephemerides of the celestial bodies to calculate the forcing, developed for degree 2, while *ARTOFS* and *HGT* use a finite number of tidal harmonics. Model data is available for limited time intervals only, not necessarily matching the intervals of gravity observations. In case of *OMCT*, the data sets were specifically calculated for this study. For the *North Sea* model, from which a very long data set is available, a suitable period based on the availability of measured SG data was chosen. The following sections discuss the properties of the different models as far as they appear of concern for the current investigation. Table 2 summarizes them in a direct comparison.
All models take the influence of sea ice into account but use different approaches (Müller et al. 2012; Arbic et al. 2012; Thomas et al. 2001; Dobslaw et al. 2013; Gräwe et al. 2019).

[1] MATLAB Releases 2014 to 2018a, The MathWorks, Inc., Natick, Massachusetts, United States.

[2] https://isdc.gfz-potsdam.de/iget-data-base/(10.07.2019)

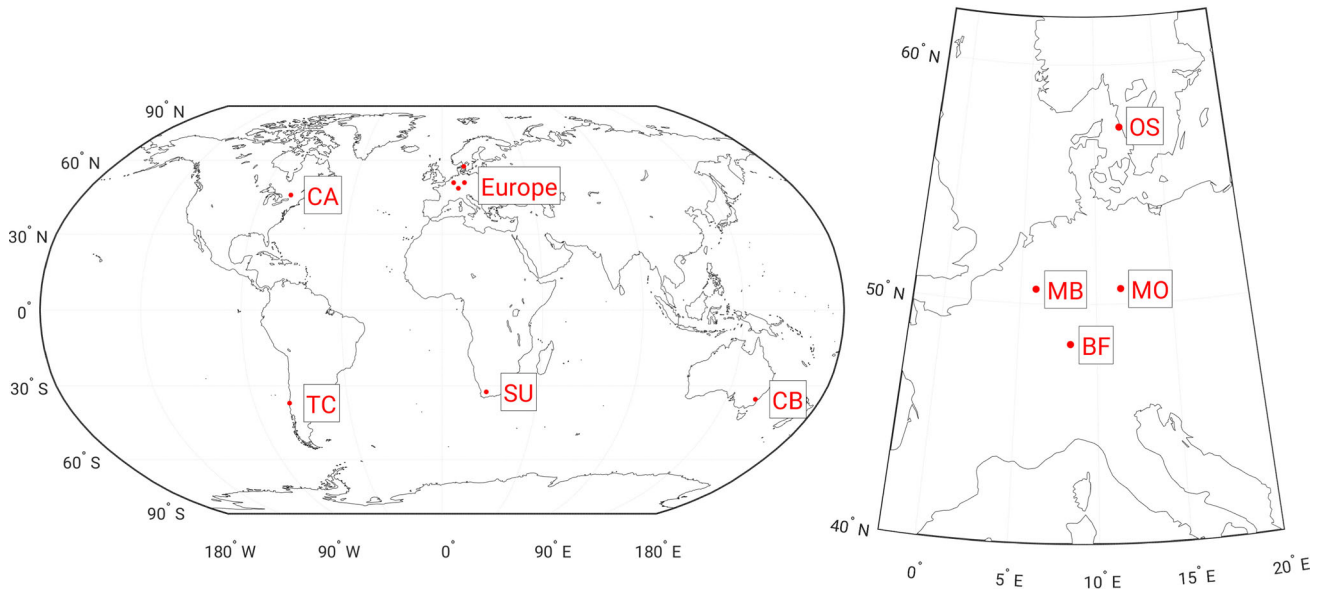

Fig. 1 Locations of the SG stations used in this study. Left: globally distributed stations, CA: Cantley, Canada; CB: Canberra, Australia; SU: Sutherland, South Africa; TC: TIGO Concepción. Right: European stations, BF: Black Forest Observatory (BFO), Germany; MB: Membach, Belgium; MO: Moxa, Germany; OS: Onsala, Sweden

Table 2 Properties of the ocean models, with ws: wind stress; wv: wind speed; p: pressure; h: heat flux; fw: fresh water flux; T: temperature; pr: precipitation; ev: evaporation; rf: radiation flux; hu: humidity; cc: cloud coverage; (c): climatologic, SSH: sea surface height; OBP: ocean bottom pressure.*: 21 isopycnal, 5 z-level.; **: different model versions available, please see Sect. 4.3 for details; ***: resolution is different in latitude and longitude direction; usage of additional data: measured or climatologically expected data are used (nudged or assimilated) in the ocean model calculation

	ARTOFS	*Stormtide*	*OMCT*	*HGT*	*North Sea*
Period	2010–2017	1954–1956	2010–2012 **	2006–2010	2009–2013
Region	North Atlantic	Global	Global	Global	North Sea
Spatial	0.03°–0.1°	0.06°	1.0°/1.875° **	0.03°	0.0333°
Resolution		0.1° ***		0.08° ***	0.0556° ***
Temporal res	1 h	1 h	2 h/3 h	1 h	1 h
Vertical layers	26*	40	20/13	32	42
Tidal forcing	8 lines	Ephemerides	Ephemerides	8 lines	–
Meteo	ws, wv, p	ws, wv	ws, p	ws, wv, p	ws, p
Forcing	fw, pr, hu	pr, hu	fw	pr, ev	fw, pr, hu
	T, rf	rf, T, h(c)	T	T, h	T, cc
Output	SSH	SSH	SSH, OBP	SSH (total, nonsteric)	SSH
Usage of add. data	Yes	Yes	Yes	No	No

4.1 The Stormtide model

Stormtide is a global model that was explicitly set up for the investigation of the AVM2ssh by Müller (2012) and Müller et al. (2014). The tidal forcing is described by the tidal potential of second degree as derived from ephemerides. The meteorological forcing is climatologic which means that values for quantities used in the forcing follow the long-term average annual cycle. This differs from the other ocean models where re-analyses of meteorological observations for the specific time interval are used for meteorological forcing. The model uses additional data sets for the sea surface temperature and salinity (Steele et al. 2001). *Stormtide* time series cover the time span 1954–1956.

4.2 The HYCOM global tides model (HGT)

The *HGT* model is described by Shriver et al. (2012), Arbic et al. (2010) and Arbic et al. (2012) and was for example used for the investigation of internal tides. In comparison to the

other global models it has the highest horizontal resolution but fewer vertical layers than *Stormtide*. Grid points exist at intervals of 0.03° in latitude and 0.08° in longitude. Grid intervals vary slightly over the globe. The model is driven by the eight diurnal and semidiurnal harmonics (Q1, O1, P1, K1, N2, M2, S2, K2) of largest amplitude.

Time series for nonsteric and total SSH are provided as a result of the computation. Steric effects are caused by thermal expansion or contraction. The change of volume, which causes changes in the SSH, is due to a corresponding change in density. The mass which is essential for the loading does not change due to steric effects and nonsteric SSH would be therefore the appropriate parameter to use for our study. However, no significant differences between the results obtained with non-steric and total SSH (see Sect. B in the Appendix) are observed. As the total SSH is the output of the other models, we show results from total SSH of *HGT* too.

4.3 The Ocean model for circulation and tides (OMCT)

OMCT for a long time was used as an ocean dealiasing product for GRACE (Gravity Recovery And Climate Experiment, Tapley et al. 2004), and is now used for studies of tidal electromagnetic signals in the oceans (e. g. Saynisch-Wagner et al. 2020). Compared to the other models, the model has the lowest spatial resolution. Two versions exist with an average resolution of 1.875° (Thomas et al. 2001) and 1.0° (Dobslaw et al. 2013), respectively. We use total SSH and ocean bottom pressure (OBP) time series as provided with samples every 3 h for the 1.875° and every 2 h for the 1° resolution. We linearly interpolated the OMCT time series to obtain hourly samples. A function provided by the Climate Data Operators (CDO)[3] (Schulzweida 2018) was used for this purpose.

The OBP results from the weight of the water column which includes SSH and also accounts for density variations. We tested both outputs of *OMCT* and discuss differences in Sect. B in the Appendix. Differences appear insignificant, which indicates a minor contribution by steric effects. As the other models provide SSH values only, we also use the SSH values for OMCT.

The effect of an ice drag implementation and the influence of nudging strength were investigated. The model runs used for these comparisons are listed in Table 3.

Changes were made regarding the ice drag, because Müller et al. (2014) pointed out that this might be a reason for the variability of the M2 amplitude in Arctic regions. In the original *OMCT* version the water could transfer momentum to the ice, but not the other way around. The formulas given by Müller et al. (2014, eq. 7) were used. With the strong nudging (tenfold larger than the weak nudging) the model was forced to follow the expected, climatologic values for the sea surface salinity from the World Ocean Atlas,[4] while in case of weak nudging the model could develop more independently.

Table 3 Properties of the different *OMCT* data sets. The first column gives the property that was changed, the 2. and 3. column the length of the data set for the two versions of *OMCT*

Property	1.875°, 3 h length	1.0°, 2 h length
Original	2010–2013	2010–2013
Ice drag	2010–2015	2010–2012
Strong nudging	2010–2013	–
Weak nudging	2010–2013	–

4.4 Atlantic real-time ocean forecast system (ARTOFS)

ARTOFS (Mehra and Rivin 2010) was developed for providing precise information for e. g. ship navigation at the North American coast. It is a regional model which covers the North Atlantic from approximately 25°S to 72°N and from 98°W to 16°E. The spatial resolution varies over the grid. The resolution is highest in the Gulf of Mexico and lowest at the African coast. In the North Sea the grid interval is about 9 km which is similar to the resolution of *Stormtide* (see Table 2).

ARTOFS is a close relative to the *HGT* model (see Sect. 4.2) but, in contrast, nudges measured data for sea surface temperature from radiometers and satellites, sea surface height via sea level anomalies from altimeter data and temperature and salinity profiles from ARGO floaters. Of all the available models it is the one that incorporates the most measurements. Tidal forcing is described by the eight major diurnal and semidiurnal harmonics (Q1, O1, P1, K1, N2, M2, S2, K2). At the open boundaries it is driven by corresponding harmonics from the TPXO6 model (Egbert and Erofeeva 2002). Hourly SSH values are used for the calculation of ocean loading. The data were downloaded from http://data.nodc.noaa.gov/opendap/ncep/rtofs/ in spring 2015. Unfortunately, this website is no longer available.

4.5 North Sea model

The *North Sea* model (Gräwe et al. 2015) is a local model with a high spatial resolution which was used for the investigation of the variability of M2 and M4 and its influence on sediment transport (Gräwe et al. 2014). It is restricted to the North Sea between about 5°W and 13°E and between about 48°N and 61°N. It has the highest spatial resolution of all

[3] https://code.mpimet.mpg.de/projects/cdo/ (05.07.2019)

[4] https://www.nodc.noaa.gov/OC5/indprod.html (04.07.2019)

the ocean models used here (approx. 1 nautical mile, which equals 0.033° to 0.056°, depending on latitude). Astronomical forcing is omitted in this regional model of the North Sea since the tidal patterns are predominantly influenced by tides entering through boundary areas, such as the English Channel. Consequently, tidal forces at the open boundaries are determined and applied based on the Oregon State University (OSU) tidal data inversion model, as described by (Egbert et al. 2010). The harmonics which were used are the largest diurnal and semidiurnal tides (Q1, O1, P1, K1, N2, M2, S1, K1), the quarter-diurnal M4 and the nonlinear tides MS4 and MN4. The output is given as hourly fields of SSH.

5 Results

We investigate the behavior of these time-stepping ocean models in three respects. Although these models contain signals of several wave groups, we always focus on the M2 signal. In the first analysis in Sect. 5.1 'Spatial distribution of AVM2ssh amplitude' we compare the global distribution of the amplitude of annual variation of the M2 admittance. Then we use the SSH of the models, compute the expected gravity loading signal at selected SG stations and run a MWA for the AVM2 as would be expected in gravity tidal analysis in Sect. 5.2 'Synthetic data MWA for the ocean models' (see Sect. 2.1) . Finally, in Sect. 5.3 'Contributions from different ocean areas', we investigate the ocean areas which predominantly contribute to the AVM2 predicted by the different models.

5.1 Spatial distribution of AVM2ssh amplitude

We follow the approach by Müller et al. (2014) to compute the amplitude of AVM2ssh at each grid point of the models. From tidal analysis of the SSH time series we obtain the tidal amplitude in meters and the Greenwich phase lag. In contrast to the phase lead estimated in the solid Earth tidal analysis (local phase), the Greenwich phase lag is not estimated relative to the local potential but to the potential at Greenwich. The harmonic analysis is carried out with the 'Tidal Heights Analysis and Prediction' program (Foreman 2004; Foreman and Henry 1989) using 146 harmonics of which 45 are main harmonics of astronomical origin and 101 are shallow water harmonics. The M2 tide and its annual variation are captured by the M2 constituent and its neighbors $\alpha 2$ and $\beta 2$, which appear at a distance to M2 of $\Delta f = \frac{1}{1\text{year}}$ in frequency.

Superimposing the harmonics $\alpha 2$, $\beta 2$ and $M2$ results in an annual modulation of the M2 amplitude and phase. Like Huess and Andersen (2001) and Müller et al. (2014) we use the following approximation for the amplitude of the AVM2ssh (see Appendix 2 in the paper by Müller et al. (2014) for details):

$$A_v \approx \sqrt{A_{\alpha 2}^2 + A_{\beta 2}^2 + 2A_{\alpha 2}A_{\beta 2}\cos((-\phi_{\beta 2} + \phi_{M2} + \Delta\phi_{AS\beta}) - (\phi_{\alpha 2} - \phi_{M2} + \Delta\phi_{AS\alpha}))} \quad (2)$$

where A_v is the amplitude of the annual variation with frequency $\omega_\mathrm{v} = 2\,\pi$ year^{-1}. ϕ_{M2} is the Greenwich phase and ω_{M2} is the angular frequency of M2. $\Delta\phi_{AS\alpha}$ and $\Delta\phi_{AS\beta}$ are the differences between the astronomical arguments of M2 and $\alpha 2$ or $\beta 2$, respectively, which are needed for the correct reference to the Greenwich phase. $A_{\alpha 2}$, $A_{\beta 2}$, and $\phi_{\alpha 2}$, $\phi_{\beta 2}$ are the amplitudes and phases for the harmonics estimated from the SSH values at a given grid point.

The results for A_v for all models used in the current study are shown in Fig. 2. For Stormtide they were taken from the paper by Müller et al. (2014). For *OMCT* the model run with the changed ice drag on a 1° grid is used (see Sect. 4.3). As the different data sets (see Sect. 4.3) show only very small differences in the results of the synthetic MWA of gravity data, we choose this data set as a representative example (see Sect. 5.2.2). The results of the harmonic analyses of the other *OMCT* models are very similar.

For all five models, amplitudes of the AVM2ssh in the expected order of magnitude (several centimeters in certain shelf areas, Müller et al. 2014) are observed. The amplitude of the AVM2ssh is, in general, similarly distributed. The AVM2ssh from *ARTOFS* and *HGT* have higher amplitudes in the North Atlantic than the AVM2ssh from *Stormtide*. The amplitudes for the *OMCT* model are distributed in a slightly different way, when compared with the *Stormtide* model. In some regions, for example the Russian coast, the amplitudes of the AVM2ssh are much smaller compared to the amplitudes in this region for *Stormtide* (few millimeters instead of several centimeters). The *North Sea* model shows an AVM2ssh amplitude comparable to the *ARTOFS* and *HGT* model and is closest to the distribution of high AVM2ssh amplitudes of *Stormtide* in the North Sea (see Fig. 8 in Appendix B). Although all five ocean models show an AVM2ssh in the expected order of magnitude the following investigations with synthetic data MWA have to show if it results in an annual variation of the gravimetric tidal parameters.

The time-invariant part of the M2 amplitude is represented by the amplitude and phase for the M2 constituent (results not shown here). We chose the HAMTIDE model (Taguchi et al. 2014) as representative for a well-established time-invariant ocean model and compare the amplitudes and phases of M2.

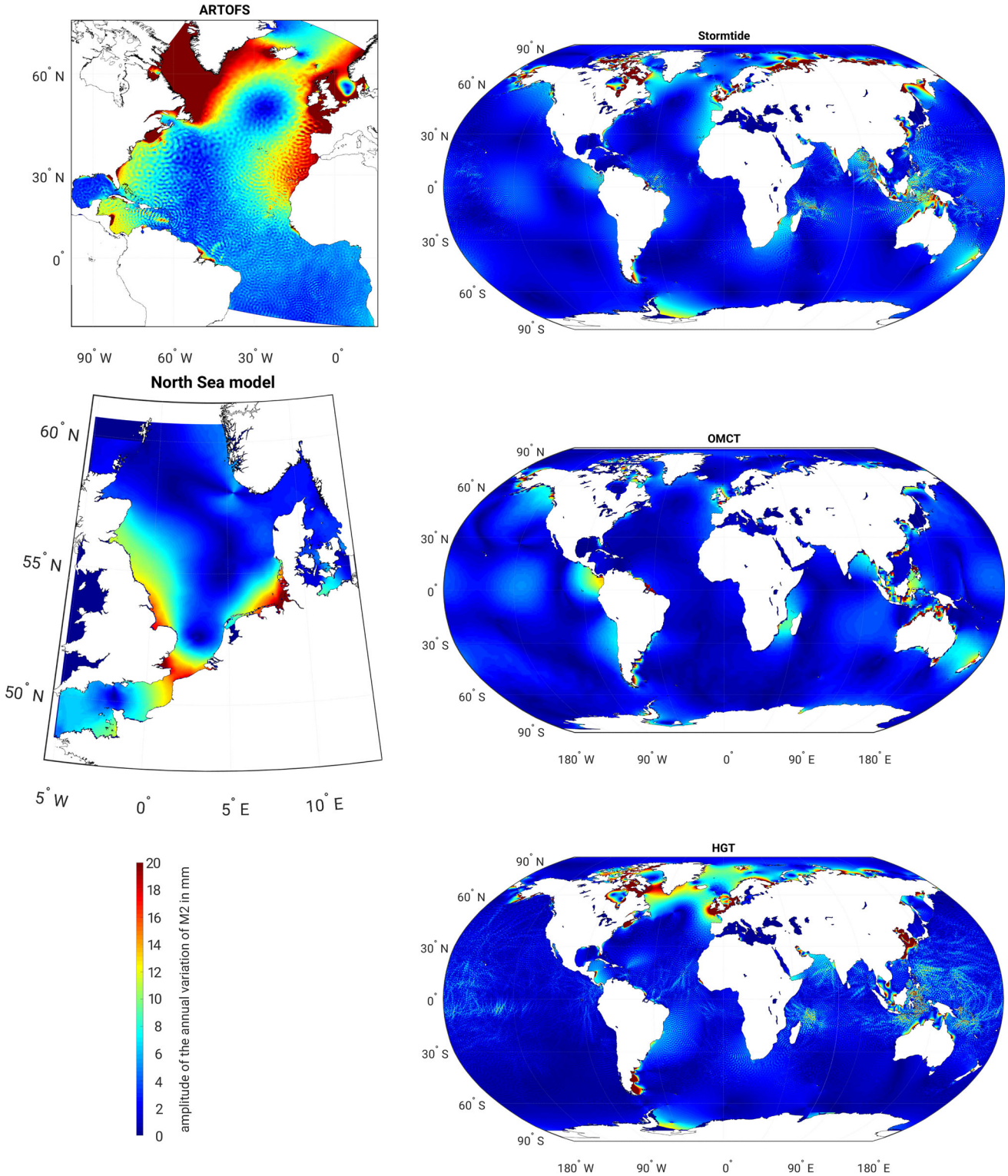

Fig. 2 Amplitudes of the annual variation of the M2 amplitude in millimeters for *ARTOFS* (top left), *North Sea* model (bottom left), *Stormtide* (top right), the *OMCT* model (center right, model run with changed ice drag), and *HGT* (bottom right). In a highly localized region, the maximum amplitude can attain approximately 30 cm. To enhance the visibility of smaller amplitude patterns along other coastlines and in the open ocean, the color scale is truncated at a maximum of 20 mm

Small differences between amplitudes and phases from the models used in this study from HAMTIDE in values and their distribution are observed (see Appendix D or sections 8.1. and 8.2.6.2 and Fig. E2-E7 given by Schroth (2019) for details). Hence the time-invariant M2 is described realistically also by the time-stepping ocean models, though not in a perfectly accurate manner (Shriver et al. 2014).

5.2 Synthetic data MWA for the ocean models

5.2.1 Comparison of the synthetic data MWA results for the ocean models

In this section the AVM2 obtained from synthetic data MWA (see Sect. 2.1) with *ARTOFS*, *Stormtide*, *OMCT*, and *HGT* loading are compared. The results for the *North Sea* model are discussed separately. For the comparison in Fig. 3 the inferred time series of tidal parameters are band-pass filtered with a lower corner frequency of 0.001cpd and a higher corner frequency of $\frac{2}{\text{year}} \approx 0.0055$cpd (see Sect. C in the Appendix for details). The tidal parameters obtained for Moxa are shown as an example. Results from other stations are available in Figs. 9 and 10 in Appendix E. To give an overview Table 5 in Appendix E lists the amplitudes of the variations shown in the above mentioned Figures. They were calculated as the mean of the half peak-to-peak amplitude of each annual period. Nevertheless this values should be regarded with caution as they are only a very rough estimate. The AVM2 does not only vary with annual period, it also contains other periods (e. g. approx. semiannual) and as it is driven by meteorology, it does not behave strictly periodic. The amplitude of the variation can differ significantly from year to year.

Figure 3 shows that loading generated by *ARTOFS*, *Stormtide* and *HGT* in an AVM2 that would be measurable by modern SG instruments. The order of magnitude of the variation is between 10^{-4} and 10^{-3} for the gravimetric factor and for phase it is 0.01° to 0.1° and matches the order of magnitude of variation in the analysis of measured gravity. The latter depends on the station (Schroth et al. 2018). The amplitude of variation of gravimetric factor obtained with loading from *HGT* at Moxa exceeds the amplitude of variation in the analysis of measured gravity by a factor of approximately 4. The extrema in the results from *HGT* and *ARTOFS* occur close (in time) to those in the measured data for both tidal parameters. The shape of the curves achieved with *Stormtide* cannot be compared directly to the results from measurements because SSH data is only available for the 1950 s. For *OMCT* no annual variations of noticeable order of magnitude occur at Moxa.

5.2.2 Comparison of *OMCT* results with different properties

The AVM2 from synthetic data MWA with *OMCT* are an order of magnitude smaller than the variations obtained with measured data. Therefore, we investigate if different model properties have a significant effect on the AVM2 (see Sect. 4.3). The results for BFO are presented as an example in Fig. 4. Results for other stations are given by Schroth (2019). Filtering is not necessary here because OMCT does not produce artifacts (see Appendix C) and we do not compare it to other models in this section.

There is no significant difference between the nudging versions and the original *OMCT* version. This is also observed for other stations (Schroth 2019). The largest difference occurs between the tidal parameters from the 1.875° and

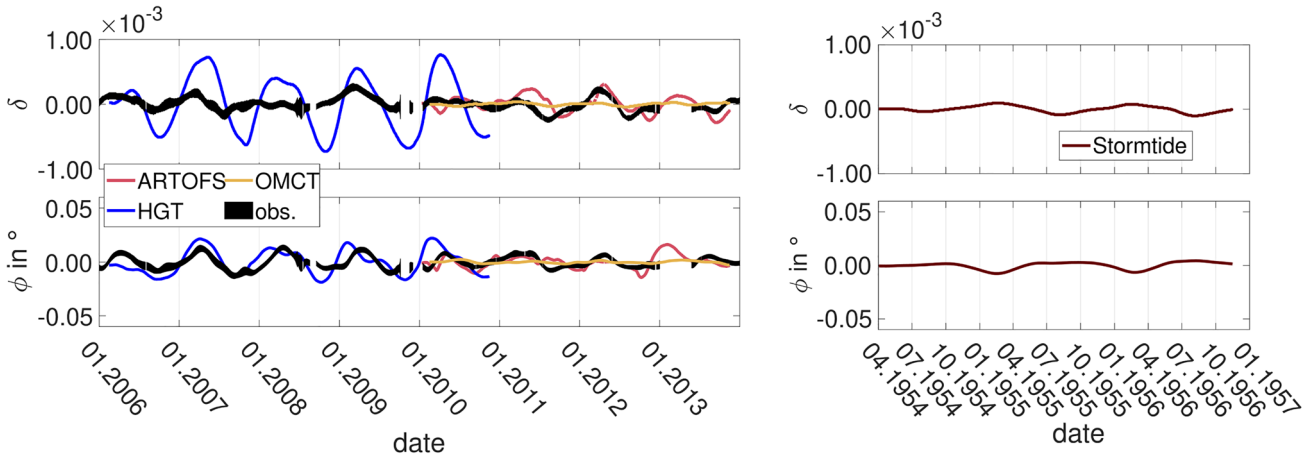

Fig. 3 Left: Tidal parameters of wave group M2 at Moxa obtained from measurements (black) and synthetic data calculated with *ARTOFS* (magenta), *OMCT* (yellow), *HGT* (blue) Right: Tidal parameters of wave group M2 at Moxa obtained from synthetic data calculated with *Stormtide* (dark-red), band-pass filtered between 0.001cpd and 0.0055cpd (see Sect. C in the Appendix

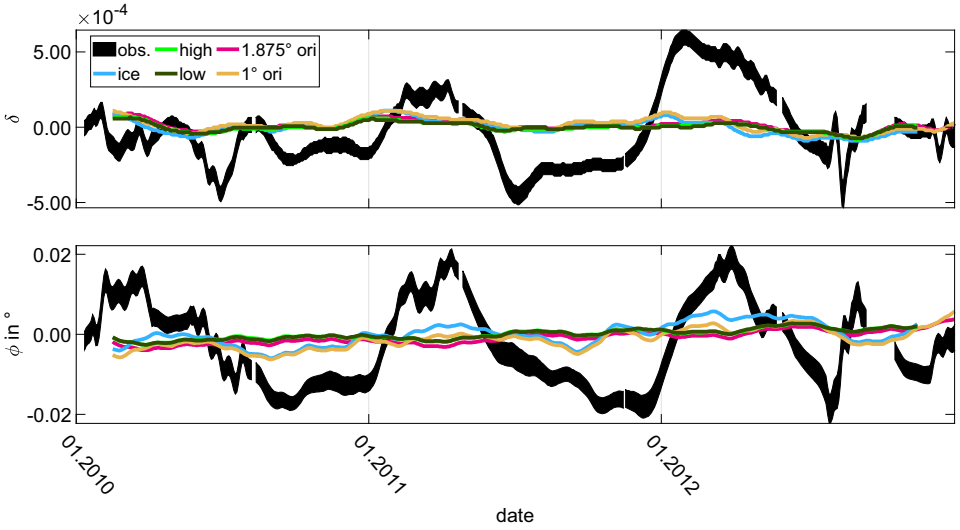

Fig. 4 Variations of the tidal parameters of the M2 wave group obtained with the *OMCT* data sets for the station BFO. The results from the measurements are shown in black. The pink curve was obtained with the SSH data set of 1.875° resolution. The light orange curve was estimated from the synthetic data calculated from the 1° version, and the cyan curve from the version with improved ice drag. The light green curve results from the high nudging and the dark green curve results from the low nudging data set. The upper panel shows the variation of the gravimetric factor, and the lower panel shows the variation of the phase in degree

the 1° version, but the AVM2 is still small compared to the AVM2 observed from measurements. There is also a small difference between the phases obtained with the version with changed ice drag and the original 1° version. However, this difference is about three times smaller than in the case of the different model resolution. Very small differences also occur for the gravimetric factors obtained with these two data sets. The variation is slightly stronger in the 1° version, suggesting that the model resolution is relevant. These results show that the tested properties (ice drag, nudging) do not affect the results significantly, if the model resolution is not high enough. This is also the case for stations close to artic regions where sea ice has probably more influence. The vertical resolution has to be high enough to resolve the processes that cause the annual variations. The 20 vertical layers in the 1° version probably cover the related effects better than the 13 layers in the 1.875° version. The relevance of the model resolution was already mentioned by others (e. g. Müller et al. 2014). However, this investigation is an additional indication that the model resolution is a dominating property. A more realistic description of other effects is of almost no influence, if the resolution is not high enough. A study of the influence of other properties should be repeated when there is a model version available with higher spatial resolution.

5.2.3 Results for the *North Sea* model

One might expect that a regional high-resolution model is able to describe the AVM2ssh in a specific ocean basin more accurately than a global model. If we assume that ocean areas close to a SG station generate a major part of the AVM2 observed at that station, the AVM2 obtained with such a kind of model should be closer to the results from observations. We use the *North Sea* model (see Sect. 4.5) to investigate this assumption for the European stations. Figure 5 shows the results for BFO and Moxa. We take these two stations as representatives because Schroth et al. (2018) show similar results for all Central European stations.

The character of parameter variation is similar for both stations and shows no AVM2. This result is surprising because the amplitudes of the AVM2ssh from the *North Sea* model (see Fig. 2) are similar to the results from *Stormtide* in the North Sea. Although the investigation in subsequent Sect. 5.3 shows that mass variations in the North Sea are not strong enough to fully explain the AVM2 at European stations. An explanation would be that the gravity contributions of the AVM2ssh from the local *North Sea* model do not sum up constructively at the analyzed stations. There are indications that the forcing of $\alpha 2$ and $\beta 2$ at the model boundaries is of significant influence (Schroth 2019), which means that the amplitudes and phases of the AVM2ssh in an ocean basin depend not just on the AVM2ssh generated in the basin, but also on the AVM2ssh propagating into the basin from neighboring regions. Further investigations are necessary to confirm this conclusion.

5.3 Contributions from different ocean areas

On the one hand, the largest amplitudes of the AVM2ssh occur in coastal areas, as shown by Müller et al. (2014) and in the results of Fig. 2 in Sect. 5.1. On the other hand, the open oceans, where the AVM2ssh has only a very small amplitude, cover large areas whose contribution could also sum up to a large amplitude in gravity.

The influence of some ocean regions on the loading that occurs at a site was studied in a way by (e. g. Baker 1980; Agnew 2001). Their conclusions are however not transferable by implication to the AVM2ssh and the AVM2. The

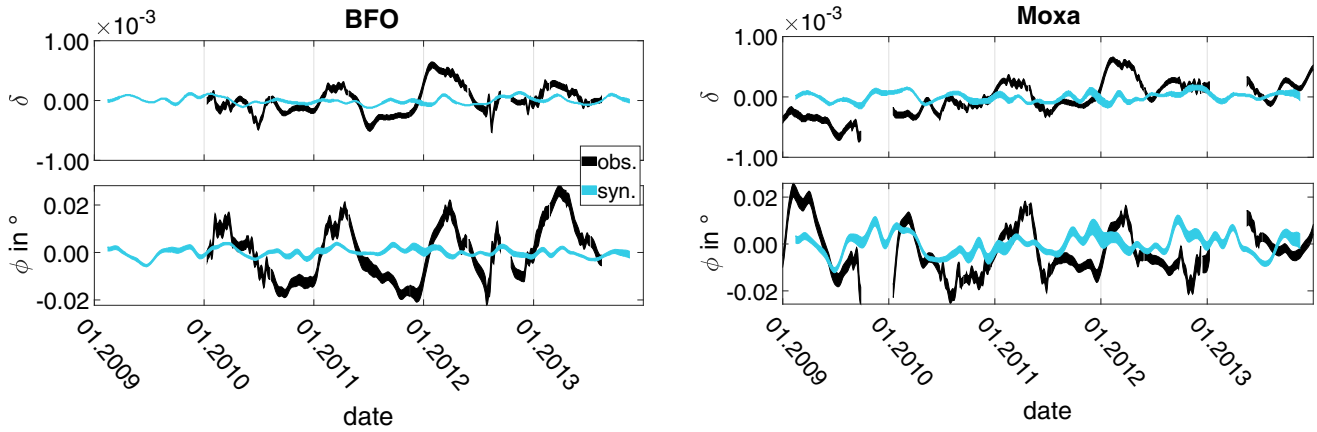

Fig. 5 Variations of the tidal parameters of wave group M2 at BFO (left) and Moxa (right) obtained from measurements (black) and synthetic data calculated with the *North Sea* model (light-blue). The mean values were subtracted

AVM2ssh is generated with a completely different mechanism and therefore could behave differently than the main tidal constituents. The amplitudes are much smaller than, e. g. the amplitude of M2.

In order to investigate which regions have to be taken into account in the loading computation so that the AVM2 at a certain station is described sufficiently well, we compute the gravity amplitude of the annual variation at every single grid point. The value $l_{\max,i}$ of gravity loading is normalized to the area $\mathrm{d}A(\vec{r}_i')$ around the grid point i, because the size of the areas may vary and also differ between the models. The value

$$\frac{l_{\max,i}(\vec{r})}{\mathrm{d}A(\vec{r}_i')} = \rho\, G(\vec{r}-\vec{r}_i')\, h(\vec{r}_i') \tag{3}$$

can be understood as areal density of gravity loading, where $\vec{r}$ is the location of the gravity sensor and $\vec{r}_i'$ is the location of grid point i. In contrast to equation 1, the values are not integrated over the Earth's surface. The amplitude of AVM2ssh is used as SSH, the phase is ignored. The resulting gravity value is, therefore, the normalized, maximal contribution $\frac{l_{\max,i}(\vec{r})}{\mathrm{d}A(\vec{r}_i')}$ to the annual variation of the M2 amplitude in gravity loading at the location of grid point $\vec{r}_i'$.

In the following, we refer to this contribution as maximum contribution or maximum gravity signal. These maximum contributions are used as thresholds for synthetic data MWA. Only grid points whose maximum gravity contribution exceeds the threshold are taken into account in a subsequent analysis of AVM2ssh loading. We compare the AVM2 produced by all grid points of the ocean model to the AVM2 obtained by excluding those grid points of the same model with a maximum gravity contribution below the regarded threshold. Subsequently the analysis proceeds with a lower threshold, which means that more grid points are considered in the loading calculation. We continue as long as the AVM2 obtained from the threshold analysis differs by more than 10% from the AVM2 obtained with the global model. This is estimated by choosing and comparing the peak-to-peak amplitudes of the AVM2 of the global model and the AVM2 with thresholds. Plotting the necessary grid points on a map will show which ocean regions contribute significant loading to gravity data at the station under consideration.

The distribution of large AVM2ssh amplitudes is similar in all models. Therefore, we run the test only with *HGT*. The stations BFO and Cantley are shown as examples here. Figure 6 shows the distribution of grid points exceeding a certain threshold for BFO and Cantley as well as the results of the corresponding analyses. Similar results for Canberra are given in Fig. 11 in Appendix E. The time varying analysis results are band pass filtered to remove artificial trends (discussed in Sect. C in the Appendix).

At BFO all grid points for which the maximum contribution exceeds $10^{-14}\,\frac{\mathrm{nm/s^2}}{\mathrm{m^2}}$ are needed to reach a deviation from the AVM2 obtained with the whole model of 10% or less. The corresponding grid points are distributed over a large region in the North Atlantic but also over distant shelf areas. The synthetic data MWA with a threshold of $10^{-12}\,\frac{\mathrm{nm/s^2}}{\mathrm{m^2}}$ at BFO shows a large phase shift compared to the results obtained from the global model. The contributions from the other regions seem to cancel out the AVM2 obtained for the higher thresholds. The variation of the gravimetric factor almost vanishes for a threshold of $5\cdot10^{-13}\,\frac{\mathrm{nm/s^2}}{\mathrm{m^2}}$. The AVM2 for the threshold of $10^{-13}\,\frac{\mathrm{nm/s^2}}{\mathrm{m^2}}$ is already relatively close to the results for the global model (but the difference is still larger than 10% for the gravimetric factor). The large AVM2 obtained for the higher thresholds are probably caused by the large amplitudes of the AVM2ssh in the North Atlantic (see Fig. 2).

In contrast to BFO, at the Cantley station, all grid points for which the maximum contribution exceeds $10^{-15}\,\frac{\mathrm{nm/s^2}}{\mathrm{m^2}}$ are necessary. These grid points are globally distributed. The investigation for the station Canberra is given in Fig. 11 in Appendix E and shows a similar behavior as Cantley. Thus, all examples show that the grid points contributing significantly to the AVM2 at the stations are distributed over the entire globe. The influence of the loading of the AVM2ssh on tidal parameters therefore has to be studied on a global scale.

6 Discussion and conclusions

The harmonic analyses of sea surface heights computed for five time stepping ocean models show that the physics implemented in contemporary modeling approaches are able to produce annual variations of the M2 sea surface amplitude in the range of several centimeters (see Sect. 5.1). This agrees well with observations from tide gauge (Müller et al. 2014; Baker and Alcock 1983) and altimeter data (Huess and Andersen 2001; Müller et al. 2014). The similarity of the general pattern (large amplitudes in dedicated shelf areas, small amplitudes in the open ocean) indicates that the models describe the principal effects causing the AVM2ssh. In detail, however, considerable differences in spatial distribution and the height of the amplitudes are observed. Calculating ocean loading from model output and analyzing the resulting time series shows that three out of the five models, namely *ARTOFS*, *Stormtide* and *HGT*, produce annual variations of the gravimetric M2 parameters at SG stations of up to 10^{-3} in the gravimetric factor and 0.1° in phase (see Sect. 5.2). These variations are of the same order of magnitude as obtained from moving tidal analyses of measured data. This is an important result, as it quantitatively confirms the hypothesis that loading by the oceans is a viable source for the observed temporal variations of tidal parameters in SG data. This conclusion, however, holds only in a general sense. The observed disparities between outcomes derived from the model and those obtained via gravimetric measurements underscore a significant limitation: current time-stepping ocean models fail to simulate the AVM2ssh accurately. This limitation aligns with expectations set by prior intercomparison of the ocean models. We have to acknowledge that the five models evaluated in this study were originally designed with diverse objectives in mind, including the prediction of sea level heights, analysis of internal tidal currents and sediment transport, and the correction of satellite gravity mission data. The discrepancy between model predictions and measured data is not surprising, because the models' main objectives do not encompass the prediction of annual variations in tidal constituents.

Based on the *HGT* model we investigated which regions of the ocean contribute significantly to the AVM2 observed at a certain station (see Sect. 5.3). At BFO, taken to represent the European stations, all grid points for which the maximum gravity contribution exceeds $10^{-14}\,\frac{\mathrm{nm/s^2}}{\mathrm{m^2}}$ are needed to reach a difference of 10% or less compared to the total AVM2. Regions of significant contributions are located in the North Atlantic and the Arctic Sea, but also at shelf regions with large amplitudes of the AVM2ssh all over the globe. For Cantley, located on the North American continent, and similar for Canberra in Australia all grid points with a maximum contribution exceeding $10^{-15}\,\frac{\mathrm{nm/s^2}}{\mathrm{m^2}}$ are necessary. In this case, grid points with significant contributions are distributed over almost the entire globe. These results imply that at BFO the shelf areas are more important than at the other two stations investigated here. Further investigations would be needed to verify this.

This analysis shows that for an accurate description of the AVM2 a global distribution of the annual variation of the M2 amplitude in the SSH is needed and a regional model such as the *North Sea* or *ARTOFS* model presumably would be insufficient.

It is particularly striking that loading contributions from shelf regions close to BFO are in direct opposition to those from distant shelves and the open ocean. This counterintuitive observation does not yet have a satisfactory explanation, indicating that compensatory contributions from other areas balance those from the shelf region near the station.

The *North Sea* model, representative of regional models, aims to delineate better the intricate patterns of AVM2ssh within bays, sounds, and straits, suggesting its utility in refining loading computations. Nevertheless, our application of the *North Sea* model did not produce an AVM2, likely due to incomplete AVM2ssh data at the model's boundaries.

The *ARTOFS* model adequately captures the regional dynamics, facilitating the generation of a synthetic AVM2 that aligns closely with observed data. It is interesting to note that the model shows an AVM2 of a similar order of magnitude as *Stormtide*, although it covers only a part of the global ocean. The investigation of the influence of different ocean areas on the AVM2 at a certain station (see Sect. 5.3) shows that *ARTOFS* contains large parts of those areas with significant contributions at European SG stations. However, the model does not include other significantly contributing regions like e. g. the Russian coast as well as distant shelf areas. Acknowledging the significant influence of distant oceanic contributions to loading raises the question of whether the amplitude of AVM2ssh represented in *ARTOFS* may be overestimated.

For the third global model, *OMCT*, the AVM2 from synthetic data MWA is an order of magnitude too low. None of the tested properties leads to an AVM2 of the correct order of magnitude. The largest (but still small) difference occurs for the 1° resolution compared to the 1.875° resolution version

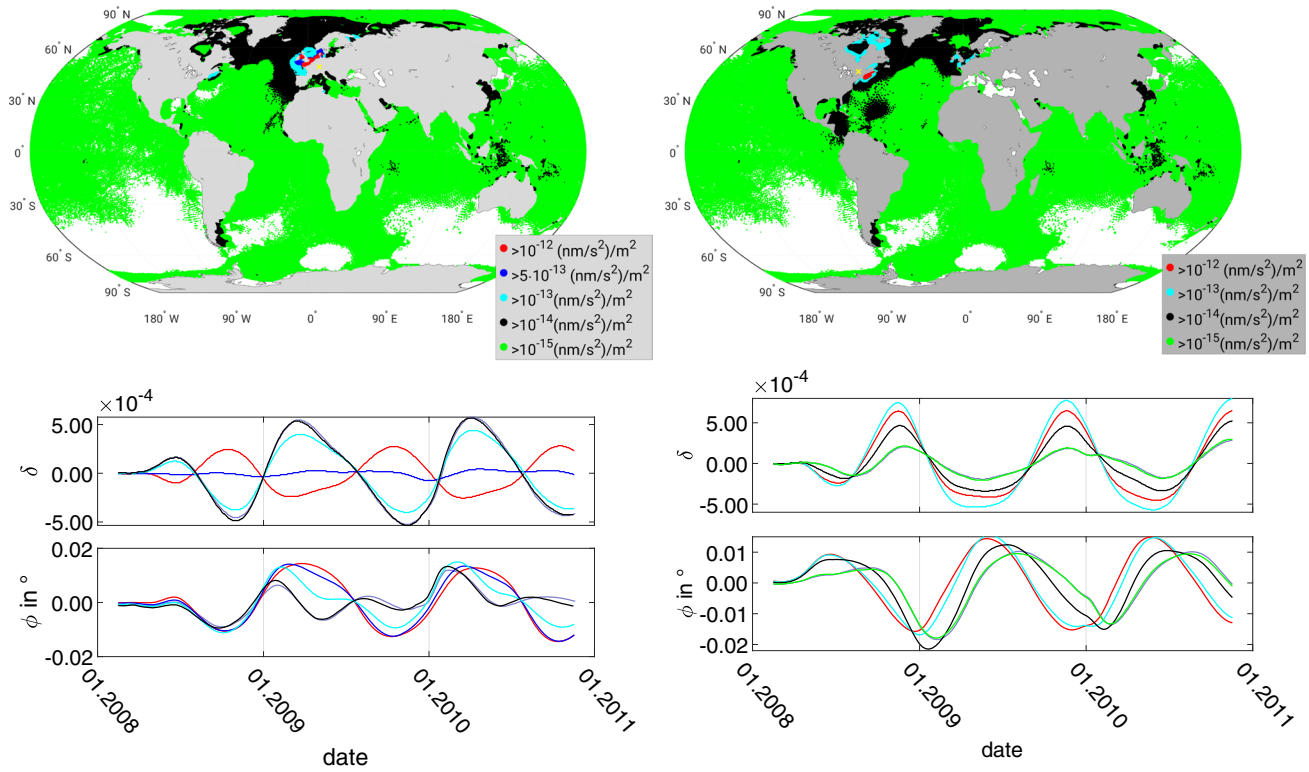

Fig. 6 Left: results for BFO. Right: Results for Cantley Top: Maps of *HGT* grid points whose gravity loading contribution exceed the threshold at the respective station. Threshold are: $10^{-12}\ \frac{\mathrm{nm/s^2}}{\mathrm{m^2}}$ in red, $5 \cdot 10^{-13}\ \frac{\mathrm{nm/s^2}}{\mathrm{m^2}}$ in blue, $10^{-13}\ \frac{\mathrm{nm/s^2}}{\mathrm{m^2}}$ in cyan, $10^{-14}\ \frac{\mathrm{nm/s^2}}{\mathrm{m^2}}$ in black and $10^{-15}\ \frac{\mathrm{nm/s^2}}{\mathrm{m^2}}$ in green. Bottom: Results of the corresponding synthetic data MWA, band-pass filtered between $\frac{1}{1000\,\mathrm{d}}$ and $\frac{2}{\mathrm{year}}$. The synthetic data MWA analysis result for the entire model is shown in light-purple. The yellow cross shows the position of the station. Please note that the synthetic data MWA is performed successively for lower thresholds until the difference to the results from the global model is equal or less than 10%. Please note that the similarity at the beginning of the curves is due to the bandpass filter

which can be taken as indication that the spatial resolution of the model is too low to represent the corresponding effects properly.

To conclude, synthetic data analysis via MWA reveals that the annual variations in oceanic M2 tides provide enough loading energy to produce the modulations observed in gravimetric M2 tides at SG stations. However, the accuracy of current ocean models in representing these variations needs to be improved for the accurate correction of gravity data for ocean loading. On the other hand, the study corroborates the ability of SG measurements in detecting sea surface height variations within the centimeter to millimeter range.

A worthwhile next step could be to study the influence of different model properties in the AVM2ssh and to use the AVM2 obtained from gravity data as a proof. In this investigation we found indications that certain model properties and phenomena are important for the occurrence of the AVM2, as already stated by others (e. g. Müller et al. 2014; Kang et al. 2002). However, we were not able to reliably identify them as relevant through comparison of the different ocean models as the models differ not only in one but in many properties. A much more detailed model study with focus on the model properties is needed to isolate and delineate specific properties which can then explain the results. The analysis of SG tidal data through narrow frequency bands presents a unique advantage, showing a marked resilience to the myriad of environmental disturbances that often compromise time series analyses. This specificity, enhanced by the lock-in effect, elevates the sensitivity of the measurements. Thus, SG stations, strategically positioned across the globe, could potentially act as a sensitive mechanism for examining the repercussions of global climate change on oceanic tidal currents. Müller et al. (2014) points out that a seasonally varying ocean stratification driven by meteorological effects and ice drag are the main causes of the annual variation of the M2 ocean tide. Both phenomena are influenced by climate change and should result in a change of the annual variability of the M2 ocean tide. Opel et al. (2024) investigate the influence of long-term changes in the stratification on tidal amplitudes based on satellite altimeter data. Such studies could profit from SG data analyses. A significant long-term effect in the variability of the M2 tidal parame-

ters is not obvious just by sight (Schroth et al. 2018). As the effect seems to be very small (Opel et al. 2024) it may show up in further investigations of the tidal parameter variations. Other climate change phenomena with small amplitude but significant influence can be identified in SG data in future investigations, offering the possibility to study and better understand these effects. Unlike tide gauges, SG technology delivers spatially comprehensive insights into height/mass fluctuations, free from the temporal or spatial aliasing challenges associated with satellite altimeter data.

SG observations hold promise for validating oceanic dealiasing products associated with current or forthcoming gravity satellite missions, such as Grace-Follow-On. These missions have the potential sensitivity to detect centimeter-level changes in sea surface heights across the global ocean.

Appendix A Glossary

admittance: response of Earth to tidal forcing as a fraction of forcing; in the context of this text, primarily due to theoretical estimates based on solid Earth models

AVM2: annual variation of the tidal parameters of the M2 tide obtained from gravity data

AVM2ssh: annual variation of the parameters of the M2 tide in sea surface height

ARTOFS: Atlantic Real-Time Ocean Forecast System

HGT: HYbrid Coordinate Ocean Model, Global Tides

OMCT: Ocean Model for Circulation and Tides

North Sea: North Sea Model

MWA: moving window tidal analysis

OBP: ocean bottom pressure

SSH: sea surface height

Appendix B Accuracy of the loading calculation

The loading calculation described in Sect. 2.3 is based on assumptions such as a constant density, which is not realistic and neglects some effects such as the height of the gravimeter station and the extent of model grid cells. The influence of these simplifications is discussed in the following.

Synthetic data MWA (see Sect. 2.1) with different density values or with output from the ocean models containing different information about density variations (SSH/OBP, *OMCT*; total/non-steric SSH, *HGT*, see Sect. 4)) resulted in insignificant differences of the AVM2. The same holds for the approximation of the model area with rectangles around the grid cells. The interpolation of the Green's functions to the required distances was found to be of significant influence only for the time-invariant part (mean value) of the tidal parameters (in the order of 10^{-3} for the gravimetric factor and 0.01° for the phase), but not for its variation.

In order to check if the altitude of the station or the extent of the model grid cells are of significant influence for the AVM2 we compare with the software package SPOTL (Agnew 2012) for the calculation of loading time series for *OMCT* (all stations) and *HGT* (BF and OS, half a year of data). Because *OMCT* is the model with the coarsest grid, the loading calculation with *OMCT* is more strongly affected than loading calculations from the other models (Olsson et al. 2009). *HGT* is the global model with the finest grid and is, therefore, less affected. The other models lie in between.

Only the time-invariable part differs when the synthetic data MWA based on SPOTL is compared to our simplified loading calculation. The only exception of that result is the synthetic data MWA with *OMCT* at Onsala, where the variation of the tidal parameter is threefold increased. Onsala is exceptional because the SG is located extremely close to the coast (in the range of hundreds of meters), where the resulting effects are considered by SPOTL but not by our computation.

For *HGT*, only 6 months of data were calculated for two stations, because the computation time for SPOTL is significantly larger. The additional required interpolation to an equidistant grid additionally contributes to the longer computation time. The AVM2 of the synthetic data MWA with loading calculated by SPOTL do not differ from the AVM2 with the simplified calculation.

For the time-invariant part of the M2 tidal parameters, the neglected effects have a smaller influence for *HGT* than for *OMCT*. A more detailed description of the mentioned analyses is given by Schroth (2019).

From the comparison with SPOTL we conclude that the approximations used in our approach do not limit the informative value of our analyses.

Appendix C Artifacts

The results presented in Figs. 3 and 6 in Sect. 5.2.1 were band-pass filtered because otherwise artifacts would obscure the AVM2 we are interested in. The following artifacts occurred in the results from synthetic data MWA:

- The tidal parameters obtained from synthetic data MWA with *ARTOFS* contain a step at the beginning of 2012 which is due to a restart of the model run because of an update of the TPX06 model which defines the tides at the model boundaries. The step was corrected with the corresponding function in the data editing software Tsoft (van Camp and Vauterin 2005).
- The *ARTOFS* tidal parameters also show short periodic (few months) variations which are most likely caused by

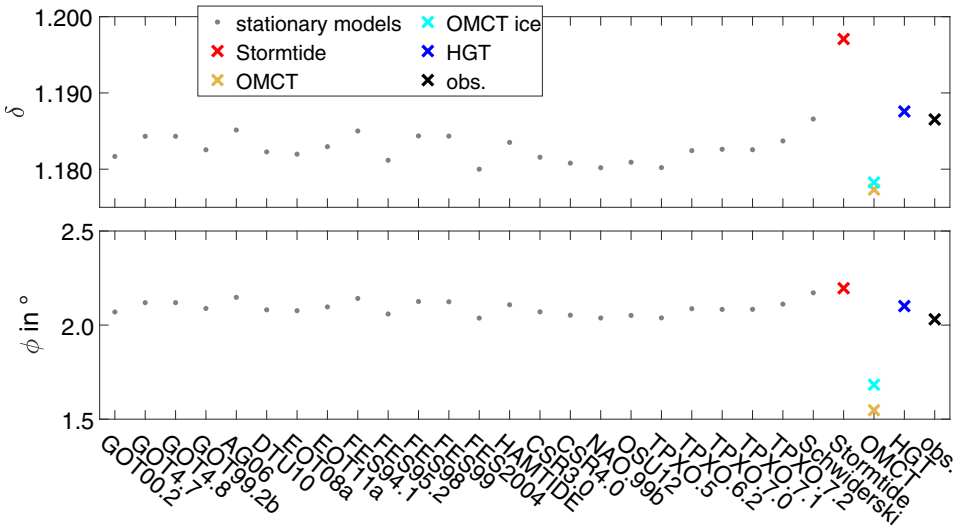

Fig. 7 Top: Gravimetric factors obtained with altimeter models[5] (gray) and the time-variable models Stormtide (red), the original 1° (light orange) and the changed ice drag version (cyan) from *OMCT* and *HGT* (blue) in comparison to the results from measurements (black). Bottom: Same for the phase. No standard deviations are shown here because they are of an order of 10^{-5} for the gravimetric factor and 10^{-3} for the phase and would be almost invisible

the model boundaries. This is indicated by a synthetic data MWA with a cutout of the model at a distance to the boundaries, in which these short-period variations were considerably reduced. Removing these short-period variations defines the upper corner frequency $f_{cu} = \frac{2}{\text{year}}$ of the band-pass filter used in Sects. 5.2.1 and 5.3.

- Artifacts occur in the results from *HGT* because the loading calculated from those models does not contain all harmonics in the M2 group. Only 8 harmonics define the tidal forcing. Only a constant nodal correction is applied, which causes a variation with a period of 18.6 years, because the analysis model contains the time dependence corresponding to this frequency. The variation vanishes if the corresponding harmonic is removed from the M2 wave group but then also the $\alpha 2$ and $\beta 2$ are excluded. The wave group being modified in this way is therefore inappropriate for studying the AVM2. The lower corner frequency ($f_{cl} = \frac{1}{1000\,\text{d}} \approx \frac{0.37}{\text{year}}$) is the lowest frequency which could be used with the given length of the time series. That *ARTOFS* does not suffer from the same problem is probably due to the nudging of measurements.

Schroth (2019) describes these artifacts in more detail.

Appendix D The time-invariant part of the tidal parameters

The time-invariant part of the tidal parameters (mean value) represents the temporally constant part of the M2 gravimetric factor or phase. The time-invariant part has the same meaning as the gravimetric factor estimated from a long data set. A deviation of the time-invariant part of the tidal parameters obtained with MWA and tidal parameters obtained from a long data set occurs if the length of the data set is not an integer multiple of the variation period.

Table 4 Definition of wave groups as given by Wenzel (1997b). The first column gives the name of the wave group, which corresponds to the largest line within the group. f_s is the start and f_e the end frequency of the wave group in cpd

Name	f_s in cpd	f_e in cpd
Q1	0.501370	0.911390
O1	0.911391	0.947991
M1	0.947992	0.981854
K1	0.981855	1.023622
J1	1.023623	1.057485
OO1	1.057486	1.470243
2N2	1.470244	1.880264
N2	1.880265	1.914128
M2	1.914129	1.950419
L2	1.950420	1.984282
S2	1.984283	2.451943
M3M6	2.451944	7.000000

The time-invariant parts of the tidal parameters obtained with the different ocean models (see Sect. 5.2.1) we compare with the results obtained with measurements and with loading calculations based on time-invariant models. We use the BFO as an example location for this analysis. The latter values are obtained from the Ocean Loading Provider[5] (OLP) by H.-G. Scherneck and M. S. Bos. It takes into account effects which are neglected in our simplified loading calculation (see Sect. 2.2 and C). The loading values obtained from OLP are used for calculating the resulting tidal parameters assuming a gravimetric factor $\delta = 1.16$ and phase $\phi = 0°$ for the solid

[5] http://holt.oso.chalmers.se/loading/index.html (05.07.19)

Table 5 Amplitudes of the AVM2 estimated by from the AVM2 shown in Figures 3, 9 and 10. They were calculated as the mean of the half peak-to-peak amplitude of each annual period

station	measured data		ARTOFS		Stormtide		OMCT		HGT	
	$\Delta\delta$ $\cdot 10^{-4}$	$\Delta\phi$ in° $\cdot 10^{-3}$	$\Delta\delta$ $\cdot 10^{-4}$	$\Delta\phi$ in° $\cdot 10^{-3}$	$\Delta\delta$ $\cdot 10^{-4}$	$\Delta\phi$ in° $\cdot 10^{-3}$	$\Delta\delta$ $\cdot 10^{-4}$	$\Delta\phi$ in° $\cdot 10^{-3}$	$\Delta\delta$ $\cdot 10^{-4}$	$\Delta\phi$ in° $\cdot 10^{-3}$
BF	0.6	6.2	1.5	10.5	0.6	4.5	0.4	1.4	4.0	5.6
BH	1.4	13.8	1.1	9.6	0.7	5.1	0.4	1.9	3.2	6.5
CA	2.7	8.6	5.9	38.2	1.6	3.2	0.5	2.4	2.3	10.0
CB	4.6	17.3	–	–	1.1	7.9	0.9	4.2	2.6	13.3
MB	2.5	5.4	1.9	12.4	0.8	6.2	0.4	2.5	4.5	19.4
MO	1.1	8.6	1.5	9.3	0.7	4.6	0.3	2.1	5.1	15.3
OS	9.9	36.6	9.5	31.6	7.4	13.3	9.8	16.4	5.7	64.2
SU	2.8	7.4	–	–	1.1	7.2	0.7	2.2	6.1	9.4
TC	3.1	21.5	–	–	2.6	12.4	2.7	6.8	1.9	10.0

Earth (see Sect. 2.1). They are given with the results for the time-variable models in Fig. 7. *ARTOFS* and the *North Sea* model are not shown here. Due to their limitation to certain areas, they cannot provide reasonable mean values.

Several issues have to be considered for the comparison. Differences of the mean values can occur for reasons other than the factors present in the ocean models. The difference of the theoretical gravimetric factors we assumed here and the values estimated for Earth models (see Sect. 3) cause a deviation of all the synthetic data MWA results from the results obtained with measurements. This difference is however orders of magnitude smaller than the deviations we can see in Fig. 7 (Dehant et al. 1999) and therefore is not significant.

As mentioned in Sect. B the time-invariant parts of the tidal parameters differ significantly due to neglected effects (see Sect. B) and different assumptions in the simplified loading calculation and SPOTL or OPL. When testing for the consequences of these simplifications, we found that they will not exceed $5.1 \cdot 10^{-3}$ in the gravimetric factors and 0.06° in the phase (for details see Schroth 2019, section 8.2.6.2). The results from the time-invariant models vary in a similar range of about $5 \cdot 10^{-3}$ (gravimetric factor) and 0.1° (phase lead). Therefore, differences of this order of magnitude between the results from time-invariant and time-variable models or between time-variable models and measurements are not interpreted.

For *OMCT* additionally the interpolation to hourly values causes mean values which are too low by $1.4 \cdot 10^{-3}$ to $2.5 \cdot 10^{-3}$ for the gravimetric factor and 0.14° for the phase. However, this cannot explain the differences between the tidal parameters of the time-invariant models and the mean values from *OMCT*.

If the mean values obtained with measured data are taken as the true values and we assume errors in the range estimated previously in this section (i. e. about $\pm 5 \cdot 10^{-3}$ in the gravimetric factor and ±0.1° in the phase), then most of the results from the time-invariant models and the results from *HGT* are within the error range. The *HGT* model describes the time-invariant part of M2 equally as well as the time-invariant ocean models, which is remarkable as *HGT* does not use any kind of nudging or assimilation.

For *Stormtide* only one of both tidal parameters is within this range. The results have a phase lead within the error range but the gravimetric factor is too large.

This investigation shows that the models used here, with the exception of *HGT*, do not explain the time-invariant M2 as accurately as time-invariant ocean models do.

Appendix E Additional information and figures

See Figs. 8, 9, 10, 11

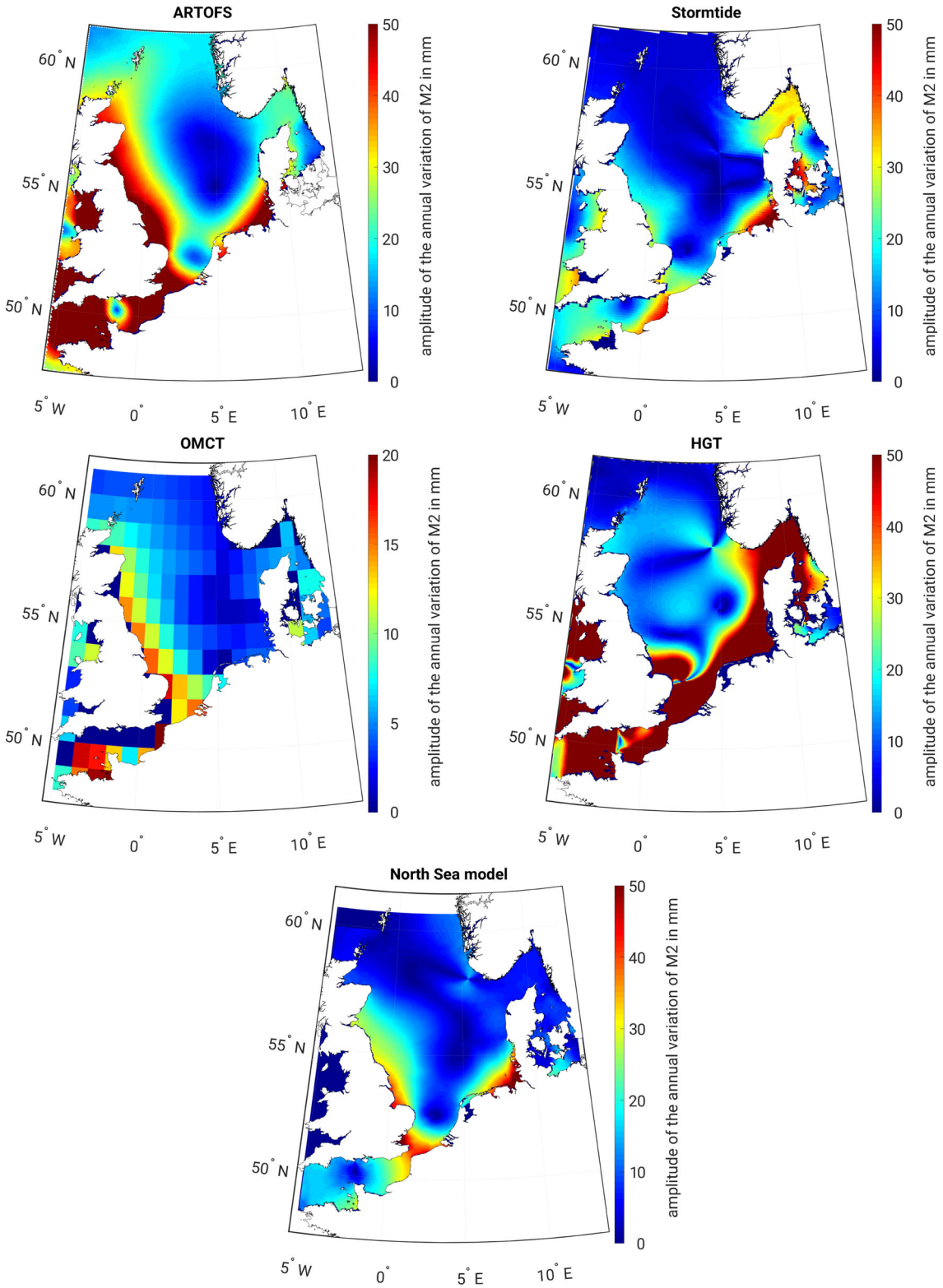

Fig. 8 Amplitude of the annual variation of the M2 amplitude from *ARTOFS* (top left), *Stormtide* (top right), *OMCT* data set with changed ice drag (center left), *HGT* (center right) and the *North Sea* model (bottom). Please note that the dark blue colors close to the coasts can be due to land grid points which have zero amplitude. Also, note the different color scale for *OMCT*; the amplitudes are also in a range of centimeters but only half of the amplitudes of the other models

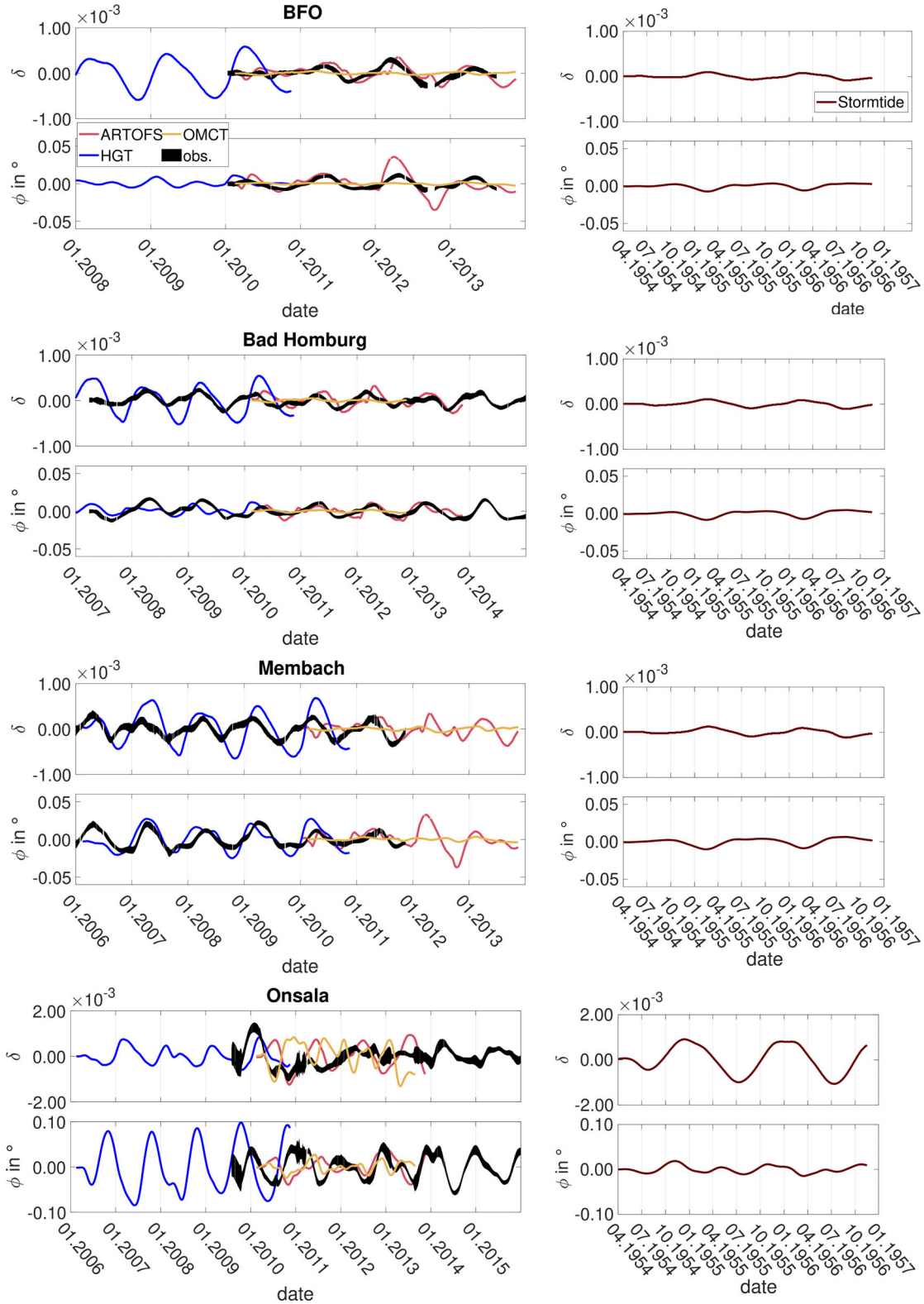

Fig. 9 Tidal parameters of wave group M2 at the European stations BFO, Bad Homburg, Membach and Onsala obtained from measurements (black) and synthetic data calculated with *ARTOFS* (magenta), *HGT* (blue), *OMCT* (yellow) (left) and *Stormtide* (dark-red, right), band-pass filtered between $\frac{1}{1000\,\mathrm{d}}$ and $\frac{2}{\mathrm{year}}$, band-pass filtered between 0.001cpd and 0.0055cpd (see Sect. C in the appendix)

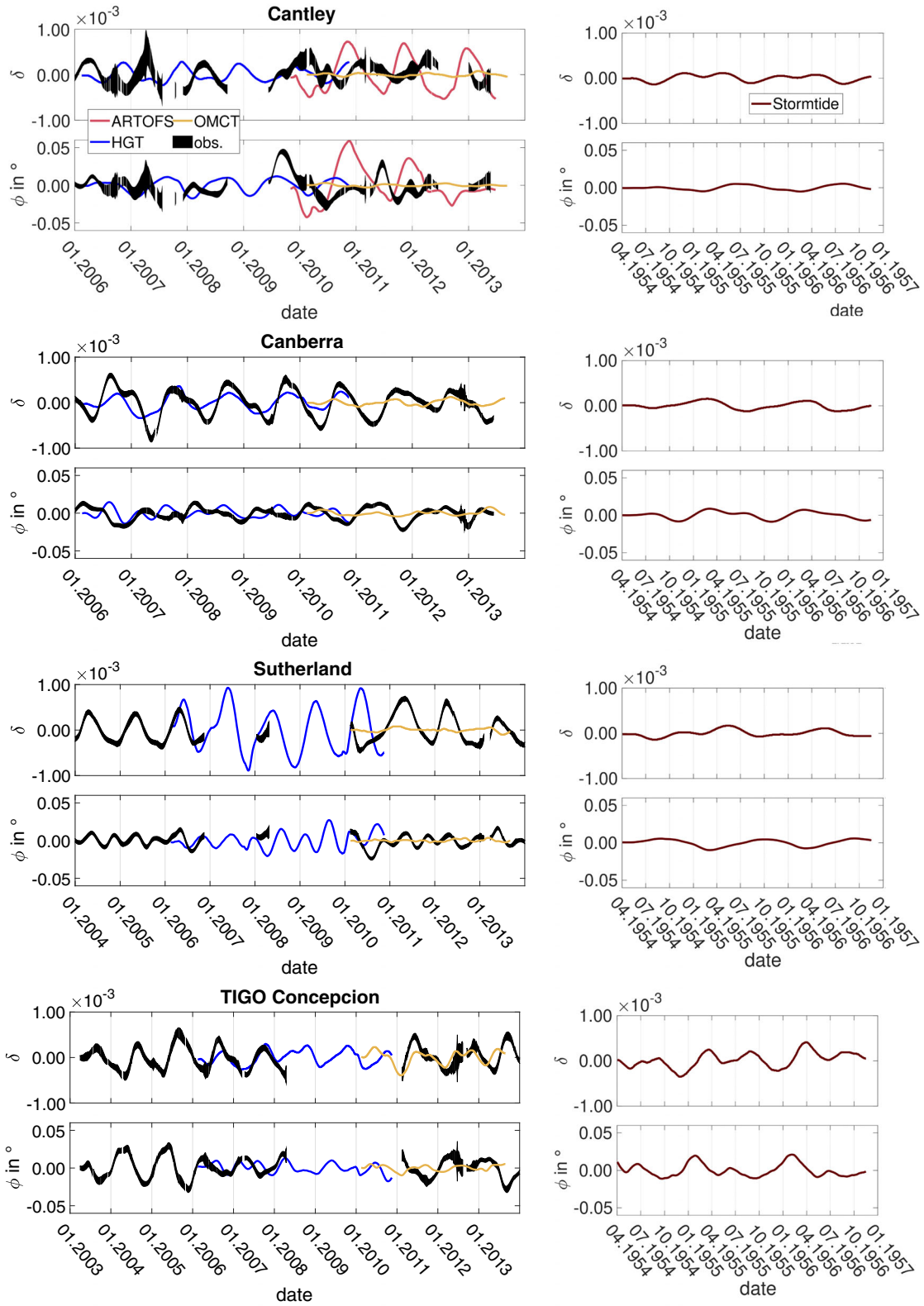

Fig. 10 Tidal parameters of wave group M2 at Cantley, Canberra, Sutherland and TIGO Concepción obtained from measurements (black) and synthetic data calculated with *ARTOFS* (magenta), *HGT* (blue), *OMCT* (yellow) (left) and *Stormtide* (dark-red, right), band-pass filtered between 0.001cpd and 0.0055cpd (see Sect. C in the Appendix)

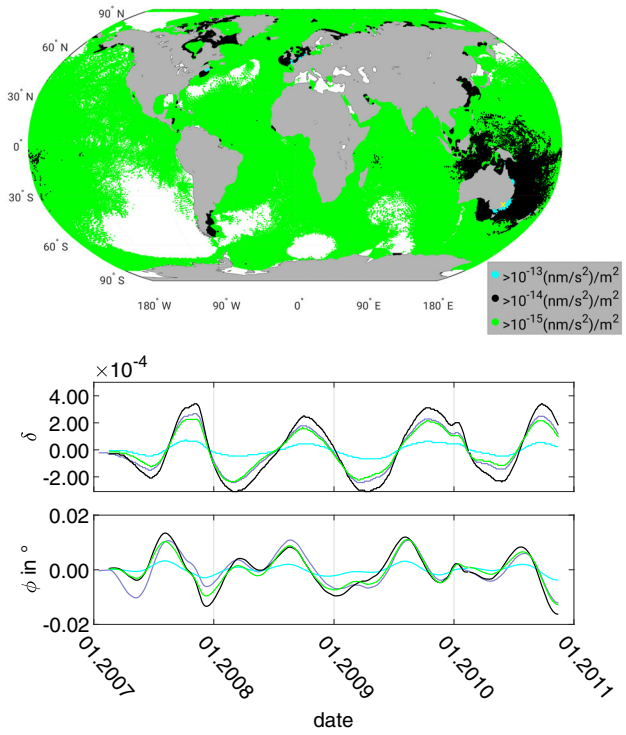

Fig. 11 Top: map of HGT grid points for which the gravity loading contribution exceeds the threshold of $10^{-12}\,\frac{\mathrm{nm/s^2}}{\mathrm{m^2}}$ in red, $5\cdot10^{-13}\,\frac{\mathrm{nm/s^2}}{\mathrm{m^2}}$ in blue, $10^{-13}\,\frac{\mathrm{nm/s^2}}{\mathrm{m^2}}$ in cyan, $10^{-14}\,\frac{\mathrm{nm/s^2}}{\mathrm{m^2}}$ in black and $10^{-15}\,\frac{\mathrm{nm/s^2}}{\mathrm{m^2}}$ in green at Canberra. Bottom: Results of the corresponding synthetic data MWA, band-pass filtered between 0.001cpd and 0.0055cpd (see Sect. C in the Appendix); the synthetic data MWA analysis result for the whole model is shown in light-purple. The yellow cross shows the position of the station. Please note that the synthetic data MWA is performed successively for lower thresholds until the difference to the results from the global model is equal or less than 10%. Please note that the similarity at the beginning of the curves is due to filtering

Acknowledgements We thank Walter Zürn and Hans-Georg Scherneck for the valuable discussions and input to the project. Liyan Liu, employed at the National Oceanic and Atmospheric Administration at that time, provided information on and help in the Atlantic Real-Time Ocean Forecast system. Thomas Hertweck helped us with his knowledge of LaTex. Hans-Georg Scherneck and Rosemary Morrow made research stays at the Onsala Space Observatory (Sweden) and at the Laboratoire des Études en Géophysique et Océanographie Spacial (France) possible for Eva Schroth. Bernhard Heck supported us with administrative tasks. The project was funded by the German Research Foundation (DFG grant WE-2628/4-1) and the Landesgraduiertenförderung Baden-Württemberg via a scholarship for Eva Schroth. All figures were created with Matlab (Releases 2014 to 2018a, The MathWorks, Inc., Natick, Massachusetts, United States).

Author Contributions E.S. implemented and carried out the data analysis and wrote the manuscript. E.S., T.F., and M.W. designed the concept of this study. K.D. assisted in the data analysis. M.M., J.-S.-W., B. K. A., M. T., U. G., J. S., and A. M. provided data from their ocean models and complemented the concept and the interpretation for the results especially regarding the ocean models. J. S.-W. ran the OMCT model in specific configurations for this study.

Funding Open Access funding enabled and organized by Projekt DEAL.

Data Availability SG data is available via the International Geodynamics and Earth tide service (Voigt et al. 2016). Ocean model time series are not publicly available. Inquiries in this regard may be directed to the authors.

Declarations

Conflict of interest The authors have no Conflict of interest to declare that are relevant to the content of this article.

References

Agnew DC (2001) Map projections to represent possible effects of surface loadin. J Geod Soc Japan 47(1):255–260 (https://www.jstage.jst.go.jp/article/sokuchi1954/47/1/47_1_255/_pdf/-char/en)

Agnew DC (2012) Spotl: Some programs for ocean-tide loading. Technical report, Scripps Institution of Oceanography, http://igppweb.ucsd.edu/~agnew/Spotl

Arbic BK, Wallcraft AJ, Metzger EJ (2010) Concurrent simulation of the eddying general circulation and tides in a global ocean model. Ocean Mod 32:175–187. https://doi.org/10.1016/j.ocemod.2010.01.007

Arbic BK, Richman JG, Shriver JF et al (2012) Global modeling of internal tides within an eddying ocean general circulation model. Oceanography 25(2):20–29. https://doi.org/10.5670/oceanog.2012.38

Baker T (1980) Tidal gravity in great britain: tidal loading and the spatial distribution of the marine tide. Geophys J R astr Soc 62:249–267. https://doi.org/10.1111/j.1365-246X.1980.tb04854.x

Baker TF, Alcock GA (1983) Time variation of ocean tides. In: Kuo JT (ed) Proceedings of the ninth international symposium on earth tides. E. Schweizerbart'sche Verlagsbuchhandlung, Stuttgart, pp 341–350, isbn: 978-3-510-65113-9

Baker TF, Bos MS (2003) Validating earth and ocean tide models using tidal gravity measurements. Geophys J Int 152:468–485. https://doi.org/10.1046/j.1365-246X.2003.01863.x

van Camp M, Vauterin P (2005) Tsoft: graphical and interactive software for the analysis of time series and earth tides. Comput Geosci 31:631–640. https://doi.org/10.1016/j.cageo.2004.11.015

Corkan R (1934) An annual pertubation in the range of tide. prsla 144:537–559. https://doi.org/10.1098/rspa.1934.0067

Dehant V (1987) Tidal parameters for an inelastic earth. Phys Earth Planet Inter 49:97–116. https://doi.org/10.1016/0031-9201(87)90134-8

Dehant V, Defraigne P, Wahr JM (1999) Tides for a convective earth. J Geophys Res 104:1035–1058. https://doi.org/10.1029/1998JB900051

Dobslaw H, Flechtner F, Bergmann-Wolf I et al (2013) Simulating high-frequency atmosphere-ocean mass variability for dealiasing of satellite gravity observations: AOD1B RL05. J Geophys Res Oceans 118(7):3704–3711. https://doi.org/10.1002/jgrc.20271

Egbert GD, Erofeeva SY (2002) Efficient inverse modeling of barotropic ocean tides. J Atmos Oceanic Technol 19:183–204. https://doi.org/10.1175/1520-0426(2002)019<0183:EIMOBO>2.0.CO;2

Egbert GD, Erofeeva SY, Ray RD (2010) Assimilation of altimetry data for nonlinear shallow-water tides: Quarter-diurnal tides of the northwest european shelf. Continental Shelf Research pp 668–679. https://doi.org/10.1016/j.csr.2009.10.011

Farrell WE (1972) Deformation of the earth by surface loads. Rev Geophys 10(3):761–797. https://doi.org/10.1029/RG010i003p00761

Foreman MGG (2004) Manual for tidal heights analysis and prediction. Pacific marine science report, Institute of Ocean Sciences, http://www.omg.unb.ca/GGE/5013_LABS/heights.pdf

Foreman MGG, Henry RF (1989) The harmonic analysis of tidal model time series. Adv Water Resour 12:109–120. https://doi.org/10.1016/0309-1708(89)90017-1

Foreman MGG, Walters R, Henry R et al (1995) A tidal model of eastern juan de fuca strait and the southern strait of georgia. J Geophys Res 100:721–740. https://doi.org/10.1029/94JC02721

Gräwe U, Müller M, Schuttelaars HM et al (2014) Seasonal variability in M_2 and M_4 tidal constituents and its implications for the coastal residual sediment transport. Geophys Res Lett 41:5563–5570. https://doi.org/10.1002/2014GL060517

Gräwe U, Holtermann P, Klingbeil K et al (2015) Advantages of vertically adaptive coordinates in numerical models of stratified shelf seas. Ocean Mod 92:56–58. https://doi.org/10.1016/j.ocemod.2015.05.008

Gräwe U, Klingbeil K, Kelln J et al (2019) Decomposing mean sea level rise in a semi-enclosed basin, the baltic sea. J Clim 32:3089–3108. https://doi.org/10.1175/JCLI-D-18-0174.1

Huess V, Andersen OB (2001) Seasonal variation in the main tidal constituent from altimetry. Geophys Res Lett 28(4):567–570. https://doi.org/10.1029/2000GL011921

Jahr T (2015) Variation der Gezeitenparameter am Geodynamischen Observatorium Moxa aus Beobachtungen mit einem supraleitenden Gravimeter. Allgemeine Vermessungs-Nachrichten 122:163–167

Kang S, Foreman MGG, Lie HJ et al (2002) Two-layer tidal modeling of the yellow ans east china seas with application to seasonal variability pf the m2 tide. J Geophys Res Oceans 107. https://doi.org/10.1029/2001JC000838

Mehra A, Rivin I (2010) A real time ocean forecast system for the North Atlantic Ocean. Terr Atmos Ocean Sci 21(1):211–228. https://doi.org/10.3319/TAO.2009.04.16.01(IWNOP)

Merriam JB (1995) Non-linear tides observed with the superconducting gravimeter. Geophys J Int 123:529–540. https://doi.org/10.1111/j.1365-246X.1995.tb06869.x

Meurers B (2004) Investigation of temporal gravity variations in SG-records. J Geodyn 38:423–435. https://doi.org/10.1016/j.jog.2004.07.011

Meurers B, Van Camp M, Francis O et al (2016) Temporal variation of tidal parameters in superconducting gravimeter time-series. Geophys J Int 205:284–300. https://doi.org/10.1093/gji/ggw017

Müller M (2012) The influence of changing stratification conditions on barotropic tidal transport and its implications for seasonal and secular changes of tides. Cont Shelf Res 47:107–118. https://doi.org/10.1016/j.csr.2012.07.003

Müller M, Cherniawsky JY, Foreman MGG et al (2012) Global m2 internal tide and its seasonal variability from high resolution ocean circulation and tide modeling. Geophys Res Lett 39. https://doi.org/10.1029/2012GL053320.2012

Müller M, Cherniawsky JY, Foreman MGG et al (2014) Seasonal variation of the m_2 tide. Ocean Dyn 64:159–177. https://doi.org/10.1007/s10236-013-0679-0

Na SH, Baek J (2011) Computation of the load Love number and the load Green's function for an elastic and spherically symmetric earth. J Korean Phys Soc 58(5):1195–1205. https://doi.org/10.3938/jkps.58.1195

Olsson PA, Scherneck HG, Ågren J (2009) Effects on gravity from non-tidal sea level variations in the baltic sea. J Geodyn 48:151–156. https://doi.org/10.1016/j.jog.2009.09.002

Opel L, Schindelegger M, Ray RD (2024) A likely role for stratification in long-term changes of the global ocean tides. Commun Earth Environ 261. https://doi.org/10.1038/s43247-024-01432-5

Sato T, Boy JP, Tamura Y et al (2006) Gravity tide and seasonal gravity variation at Ny-Alsund, Svalbard in Arctic. J Geodyn 41:234–241. https://doi.org/10.1016/j.jog.2005.08.016

Saynisch-Wagner J, Julien B, Hornschild A et al (2020) Tide-induced magnetic signals and their errors derived from CHAMP and Swarm satellite magnetometer observations. Earth, Planets and Space 73(234 (2021)). https://doi.org/10.1186/s40623-021-01557-3

Schroth E (2013) Analyse von Gezeitenregistrierungen des Supraleitenden Gravimeters SG-056. Diplomarbeit, Karlsruhe Institute of Technology (KIT), http://nbn-resolving.org/urn:nbn:de:swb:90-466565

Schroth E (2019) Analysis of temporal variations of gravimetric tidal parameters. PhD thesis, Karlsruhe Institute of Technology (KIT), https://doi.org/10.5445/IR/1000123241, https://katalog.bibliothek.kit.edu/cgi-bin/koha/opac-detail.pl?biblionumber=1211245

Schroth E, Forbriger T, Westerhaus M (2018) A catalogue of gravimetric factor and phase variations for twelve wave groups. KIT Scientific Working Papers 101. https://doi.org/10.5445/IR/1000089609, https://katalog.bibliothek.kit.edu/cgi-bin/koha/opac-detail.pl?biblionumber=1123887&query_desc=Schroth

Schulzweida U (2018) Climate data operators (CDO) User Guide, Version 1.9.3. https://code.mpimet.mpg.de/projects/cdo/embedded/cdo.pdf

Shriver JF, Arbic BK, Richman JG et al (2012) An evalutation of the barotropic and internal tides in a high-resolution global ocean circulation model. J Geophys Res Oceans 117(C10). https://doi.org/10.1029/2012JC008170

Shriver JF, Richman JG, Arbic BK (2014) How stationary are the internal tides in a high-resolution global ocean circulation model? J Geophys Res Oceans 119(5):2769–2787. https://doi.org/10.1002/2013JC009423

Steele M, Morley R, Ermold W (2001) A global hydrography with a high quality arctic ocean. J Clim 14:2079–2087

Taguchi E, Stammer D, Zahel W (2014) Inferring deep ocean tidal energy dissipation from the global high-resolution data-assimilative hamtide model. J Geophys Res Oceans 119:4573–4592. https://doi.org/10.1002/2013JC009766

Tapley BD, Bettadpur S, Ries JC et al (2004) Grace measurements of mass variability in the earth system. Science 305:503–505. https://doi.org/10.1126/science.1099192

Thomas M, Sündermann J, Maier-Reimer E (2001) Consideration of ocean tides in an OGCM and impacts on subseasonal to decadal polar motion excitation. Geophys Res Lett 28(12):2457–2460. https://doi.org/10.1029/2000GL012234

Voigt C, Förste C, Wziontek H et al (2016) Report on the data base of the international geodynamics and earth tide service (igets). Scientific

Technical Report STR – Data 16/08. https://doi.org/10.2312/GFZ.b103-16087

Wenzel HG (1996) The nanogal software: Earth tide data processing package ETERNA 3.30. Bulletin d'Information des Marées Terrestres 124:9425–9439

Wenzel HG (1997a) Analysis of earth tide observations. In: Wilhelm H, Zürn W, Wenzel HG (eds) Tidal phenomena, Lecture notes in earth sciences, vol 66. Springer, Berlin, pp 59–75, https://doi.org/10.1007/BFb0011457

Wenzel HG (1997b) Eterna 3.40, Manual. Black Forest Observatory, Universtät Karlsruhe, Karlsruhe, https://radar.kit.edu/radar/en/dataset/eRVHsFpMkpMrFARQ#

Wenzel HG, Forbriger T, Zürn W et al (2022) Eterna - programs for tidal analysis and prediction. Software package, Karlsruhe Institute of Technology, https://doi.org/10.35097/746

Westerhaus M (1997) Tidal tilt modification along an active fault. In: Wilhelm H, Zürn W, Wenzel HG (eds) Tidal phenomena, Lecture notes in earth sciences, vol 66. Springer, Berlin, pp 311–339, https://doi.org/10.1007/BFb0011469

Zürn W, Forbriger T, Widmer-Schnidrig R (2008) Magnetfeldeinflüsse auf Doppelkugel-Supraleitgravimeter, presentation at the annual conference of the Arbeitskreis Geophysik Geodäsie in Hirschegg